

# ULRR

## Ultrashort laser sintering of printed silver nanoparticles on thin, flexible, and porous substrates

Item Type	Article
Authors	Sharif, Ayesha;Farid, Nazar;McGlynn, Peter;Wang, Mingqing;Vijayaraghavan, Rajani K;Jilani, Asim;Leen, Gabriel;McNally, Patrick J.;O'Connor, Gerard M.
Citation	Journal of Physics D: Applied Physics, 2023, 56 (7)
Publisher	IOP Science
Download date	2026-04-23 00:38:54
Item License	<a href="https://creativecommons.org/licenses/by-nc-sa/4.0/">https://creativecommons.org/licenses/by-nc-sa/4.0/</a>
Link to Item	<a href="https://doi.org/10.34961/researchrepository-ul.23909838">https://doi.org/10.34961/researchrepository-ul.23909838</a>

PAPER • OPEN ACCESS

# Ultrashort laser sintering of printed silver nanoparticles on thin, flexible, and porous substrates

To cite this article: Ayesha Sharif *et al* 2023 *J. Phys. D: Appl. Phys.* **56** 075102

View the [article online](#) for updates and enhancements.

## You may also like

- [Experimental analysis of a low controlling voltage tri-electrode MEMS electrostatic actuator for array applications](#)  
Mehdi Allameh, Yu Zhou, Tao Chen et al.
- [A mathematical framework for nonlinear wavefront reconstruction in adaptive optics systems with Fourier-type wavefront sensing](#)  
Victoria Hutterer, Andreas Neubauer and Julia Shatkhina
- [Beam optics studies for a novel gantry for hadron therapy](#)  
E Felcini, G Frisella, A Mereghetti et al.

# Ultrashort laser sintering of printed silver nanoparticles on thin, flexible, and porous substrates

Ayesha Sharif<sup>1,2,\*</sup> , Nazar Farid<sup>1</sup> , Peter McGlynn<sup>1</sup>, Mingqing Wang<sup>3</sup> , Rajani K Vijayaraghavan<sup>4</sup> , Asim Jilani<sup>5</sup> , Gabriel Leen<sup>6,7</sup> , Patrick J McNally<sup>4</sup> and Gerard M O'Connor<sup>1,2</sup>

<sup>1</sup> National Centre for Laser Applications (NCLA), Physics, University of Galway, Galway, Ireland

<sup>2</sup> I-Form, The SFI Research Centre for Advanced Manufacturing, National Centre for Laser Applications (NCLA), Physics, University of Galway, Galway, Ireland

<sup>3</sup> Institute for Materials Discovery, University College London, London, United Kingdom

<sup>4</sup> I-Form, The SFI Research Centre for Advanced Manufacturing, Advanced Processing Technology Research Centre (APT), School of Electronic Engineering, Dublin City University, Glasnevin, Dublin 9, Ireland

<sup>5</sup> Center of Nanotechnology, King Abdul-Aziz University, Jeddah, Saudi Arabia

<sup>6</sup> PolyPico Technologies Ltd, Unit 10, Airways Technology Park, Rathmacullig West, Cork, Ireland

<sup>7</sup> Department of Electronic & Computer Engineering, University of Limerick, Limerick, Ireland

E-mail: [a.sharif1@nuigalway.ie](mailto:a.sharif1@nuigalway.ie)

Received 3 October 2022, revised 25 December 2022

Accepted for publication 16 January 2023

Published 31 January 2023



## Abstract

The fabrication of low-cost and mechanically robust flexible electronic patterns has increasingly gained attention due to their growing applications in flexible displays, touch screen panels, medical devices, and solar cells. Such applications require cost-effective deposition of metals in a well-controlled manner potentially using nanoparticles (NPs). The presence of solvent and precursors in NP based inks impacts the electrical conductivity of the printed pattern and a post-processing heating step is typically performed to restore the electrical properties and structure of the material. We report printing with picolitre droplet volumes of silver (Ag) NPs on flexible substrates using an acoustic microdroplet dispenser. The low-cost, controlled deposition of Ag ink is performed at room temperature on photopaper, polyimide and clear polyimide substrates. A localized, ultrashort pulsed laser with minimal heat affected zone is employed to sinter printed Ag patterns. For comparison, oven sintering is performed, and the results are analysed with scanning electron microscopy, four-point probe and Hall measurements. The femtosecond laser sintering revealed highly organized, connected nanostructure that is not achievable with oven heating. A significant decrease in sheet resistance, up to 93% in Ag NPs on clear polyimide confirms the laser sintering improves the connectivity of the printed film and as a result, the electrical properties are enhanced. The surface morphology attained by the laser sintering process is interpreted to be due to a joining of NPs as a result of a solid-state diffusion process in the near surface region of NPs.

\* Author to whom any correspondence should be addressed.



Original content from this work may be used under the terms of the [Creative Commons Attribution 4.0 licence](https://creativecommons.org/licenses/by/4.0/). Any further distribution of this work must maintain attribution to the author(s) and the title of the work, journal citation and DOI.

Supplementary material for this article is available [online](#)

Keywords: Ag nanoparticles, acoustic micro-droplet printing, electrical conductivity, laser sintering, femtosecond laser, oven sintering, SEM

(Some figures may appear in colour only in the online journal)

## 1. Introduction

While nanomaterials and nanostructures have been used for centuries, it is only in the last 100 years or so that it was discovered that a reduction in size to the scale of nanometres results in a dramatic change in the chemical and physical properties which differ from those of the bulk materials [1]. Nanoparticles are solid particles or particulate dispersions with sizes in the range of 1–100 nm [1]. Metallic NPs have gained much more interest due to their attractive properties including high surface area to volume ratio, low sintering temperatures due to shape and size dependant melting point depression, stability and the collective electron oscillations enabling surface plasmon resonance effects [2–5].

Among various metallic NPs, Ag NPs are of great importance due to their favourable properties including high electrical conductivity, highly efficient antimicrobial activities, high reactivity, and cost-effectiveness [6–8]. The relatively low cost of Ag compared to gold is the major factor enabling its use in large scale production and in sustainable manufacturing. Ag NPs offer promising applications in biomedicine, food packaging, optoelectronics, flexible electronics, sensing, self-disinfecting textiles, and cosmetic products [6, 9–11]. The physiochemical properties such as composition, surface coating, release of Ag<sup>+</sup> ions, size, and shape of the Ag NPs are the primary reasons for their excellent biomedical applications. Ag NPs are extensively used in various biomedical fields due to their precise interactions with the cells [12, 13]. Ag NPs serve as antimicrobials, antivirals, sterilizers, and antibacterial agents since the large surface area of the NPs allows a better contact with the microorganisms [13–15]. The incorporation of NPs in wound healing dressing has gained considerable attention in recent years. Wound dressings functionalized with Ag NPs are another therapeutic approach to develop NP dressings for wound healing [16, 17]. Other than the biomedical applications, Ag NPs are extensively used in printed and wearable electronics as patterns, electrodes, sensors and antennas [18]. The current research work is a contribution in the broad category of flexible printed electronics. The nanoscale properties of Ag NPs can significantly enhance the trapping of light due to surface plasmonic effects when incorporated in the interface between the metal and dielectric contacts in thin film solar cells [19, 20]. The multilayer patterning of Ag NPs combined with laser sintering and laser ablation was demonstrated for the fabrication of a microcontroller unit [21]. Printed materials are the best example of how the technology can be used to deposit the material in an accurate and controlled manner. The deposition of NPs can be carried out in many ways. Different droplet-based techniques have been

used to transfer the inks to desired substrates including inkjet, spray, aerosol jet and electrohydrodynamic jet-based methods [22–24]. For a cost-effective printing, it is important to reduce the ink volume with minimum waste. The droplet volume requirements have reduced from microliters to picolitres as the technology evolves making the process more efficient and cost-effective [25]. For example, a commercially available PolyPico dispensing head is able to dispense picolitre droplet volumes of Ag ink. The actuator assembly comprised of one or more piezo elements couples the acoustic energy to the ink solution in the disposable cartridge (tip), causing a drop-on-demand, non-contact ejection of liquid through the orifice [26]. This allows low-cost printing with minimal cross contamination.

Generally, functional NP inks consist of metal NP dispersions in the solvents. To avoid the aggregation of these NPs in the dispersion, metal particle-binding thiols and polymers (capping agents) are used as stabilizing agents [27, 28]. After printing, the metal NPs do not exhibit the optimal electrical properties due to the presence of stabilizing agents/solvents. The bond between the particles and the ligands must be broken to remove the polymeric ligands since the presence of an organic layer (even few nanometres thin) can hinder the mobility of electrons between the metal particles [27]. The removal of polymeric ligands results in the growth of metal-to-metal atomic diffusion by restoring the electrical conductivity of the printed pattern.

The post treatment after droplet transfer to the substrate is usually comprised of (a) a drying step and (b) a sintering step. After deposition of NP inks, the printed patterns are dried using an oven, hot plate, IR radiation or intense pulsed light to evaporate the liquid components (solvent) before sintering [29]. Therefore, the post-processing sintering step is important to build a metal-to-metal contact for desired electrical conductivity. Sintering of printed patterns is generally performed with thermal [30, 31], intense pulsed light [32, 33], plasma [24, 34, 35], electrical [36, 37] and laser sintering processes [38–43]. Thermal sintering is not suitable for many polymer substrates since they are highly sensitive to heat. Among all these methods, laser has emerged as a powerful tool for rapid and selective material processing with localized energy distribution. The pulse duration is the most important parameter that impacts the nature of laser material interactions and its associated effects. For example, in a continuous wave (CW) laser sintering, the metal NPs are fully melted and resolidify due to a relatively longer laser exposure time [30, 39, 44]. Nanosecond lasers are widely used for sintering [39, 45, 46] and facilitate the sintering process through a thermal mechanism. The thermal damage, large heat affected zone and low resolution

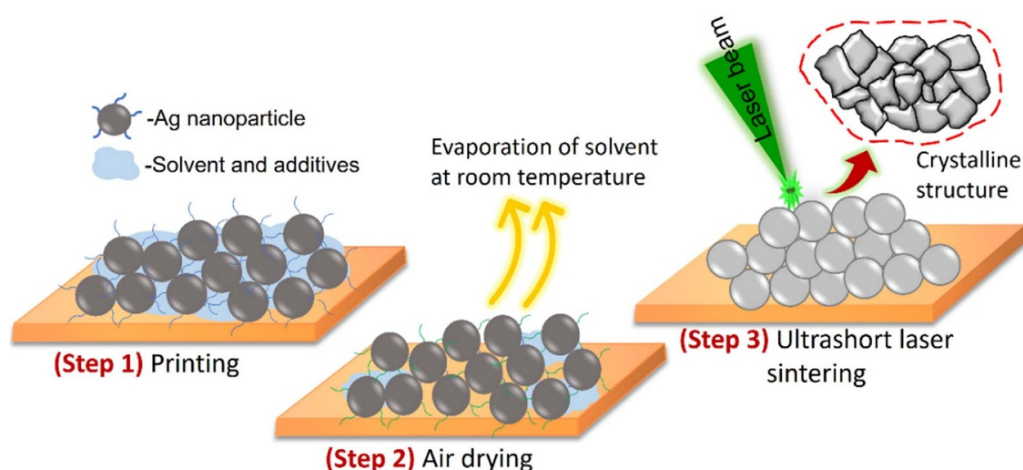


**Figure 1.** Schematic illustration of experimental strategy involving Ag NP printing, air drying at room temperature and femtosecond laser sintering steps.

caused by a CW and nanosecond lasers are not desirable for sintering of metal NPs films on heat sensitive materials. Ultrashort lasers have great potential since the pulse duration is much shorter than the duration of electron–lattice relaxation processes resulting in a non-equilibrium two-temperature phenomenon in the material, well described by a two-temperature model [47, 48]. The highly localized energy distribution can significantly reduce the heat affected zone as observed in the case of ultrashort lasers. However, the field of sintering with ultrashort lasers is relatively under-reported compared to nanosecond and CW laser techniques. The physics of ultrashort pulsed laser sintering is not fully understood as the formation of nanostructures, properties of sintered NP films on different substrates under different processing conditions, and their correlation are still ambiguous.

In this paper, we report a low cost, selective printing of Ag NPs on thin, flexible, and porous substrates using disposable cartridges that utilize a volume of  $\sim 90 \mu\text{l}$  to print many patterns with a single fill. The aim of the current study focuses on using low temperature sintering to (a) obtain highly conductive Ag patterns and (b) to prevent the thermal effects on future heat sensitive substrates. This is achieved by using femtosecond laser pulses to tune the electrical and structural properties of printed Ag films on photopaper, polyimide (PI) and clear PI substrates, respectively, with selective laser sintering. Two polyimide materials are selected as one (Hayaline) is more transparent or clear, allowing higher light transmission than the other PI (Kapton). These two materials have different optical, physical, and electrical properties. It is worthwhile investigating the impact of the substrate on the printing behaviour of NP ink, structural evolution of printed NPs, electrical properties, and sintering behaviour. The surface morphologies are analysed with scanning electron microscopy (SEM) and a correlation with the electrical properties is established. For comparison, oven sintering is performed at two different temperatures and for heating durations of 20 and 40 min, respectively. The schematic illustration presented in figure 1 depicts the experimental strategy adopted for current investigation.

**Table 1.** The specifications of the substrate material used for printing process.

Substrates	Specifications		
	Manufacturer	Thickness	Grade
Photopaper	Q-CONNECT	280 $\mu\text{m}$	Gloss-180 GSM
Polyimide	Goodfellow	50 $\mu\text{m}$	DuPont™ Kapton® FPC
Clear polyimide	Zymergen	50 $\mu\text{m}$	HAYALINE Z2

## 2. Experimental details

### 2.1. Materials

The commercially available Ag NP ink of 36% Ag wt. concentration (Dycotec Materials, UK) is used in the experiments. The viscosity of the ink was 16 cP; the surface tension was  $33.6 \text{ mNm}^{-1}$ . Three different substrates were selected for the current study including photopaper, PI and clear PI. The specifications of the substrate are listed in table 1.

### 2.2. Surface treatment and printing

When using polymer surfaces to receive the ink deposition, it is important to carry out surface treatments to improve the adhesion and surface functionalisation. The polymer substrates were subjected to argon (Ar) ion plasma treatment (kINPen Med) before printing. The plasma treatment is carried out using a plasma pen. The plasma tool was adjusted at a setting of 3.25 bar Ar gas pressure with a gas flow rate of 5–6 standard liters per minute (slm). The distance between the plasma pen nozzle and the sample surface was optimized to  $\sim 2 \text{ mm}$  to receive the maximum exposure of the plasma on the surface. The samples were scanned at a scanning speed  $270 \text{ mms}^{-1}$  with  $0.1 \text{ mm}$  hatching. To facilitate the low cost and low volume printing, a micro-dispenser head (PolyPico

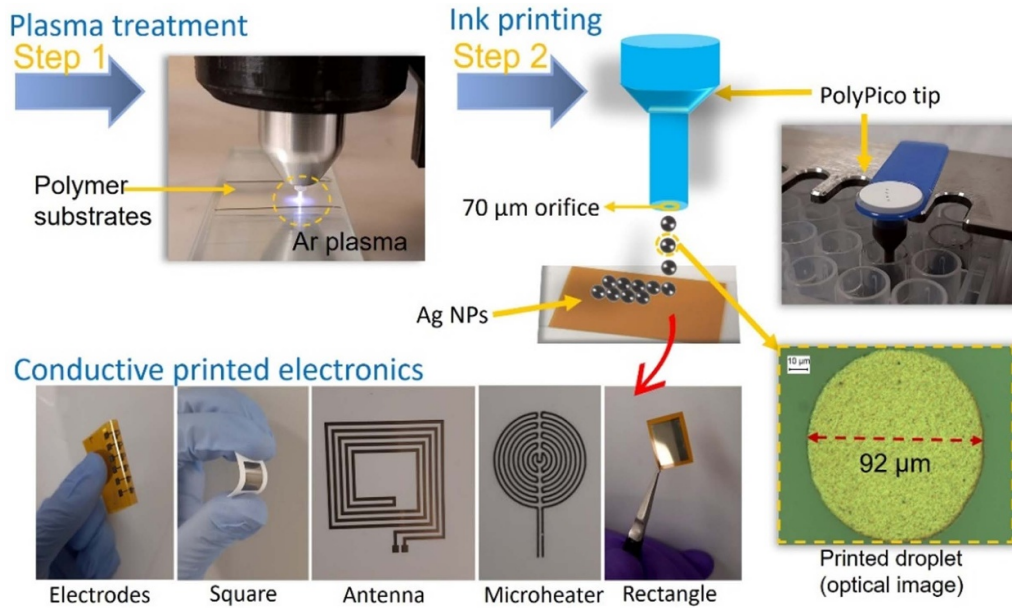


**Figure 2.** The experimental steps involved in Ag ink printing process; (Step 1) Argon gas cold plasma pre-processing of polymer for enhanced functionalization. After plasma treatment, the polymer substrate is subjected for printing (Step 2) using PolyPico microdispensing head. The droplet size of printed Ag ink using 70 μm tip size is 92 μm.

**Table 2.** Optimized print parameters used for Ag ink printing on different substrates.

Material	Print speed (mm s <sup>-1</sup> )	Separation between drops (mm)	Hatch (mm)	Frequency (Hz)
Photopaper	15	0.075	0.07	200
Polyimide	21	0.105	0.08	200
Clear Polyimide	23	0.115	0.09	200

Technologies Ltd) was used. This system utilizes acoustic energy to precisely dispense pico-litre volumes of Ag ink from the dispensing cartridge [25]. A disposable dispensing cartridge of 70 μm orifice size at 200 Hz jetting frequency was used. The printing speeds and hatching between two consecutive print lines were optimized depending upon the type of the substrate used to print square areas (9 mm × 9 mm) as shown in figure 2. The printing parameters are listed in table 2. The printed Ag patterns were dried in air at room temperature for over 24 h and later subjected to sintering.

### 2.3. Sintering

A femtosecond laser (S-Pulse Amplitude Systems) is employed as a sintering tool with a wavelength in the visible region of the electromagnetic spectrum. The laser pulse duration is 500 fs, at a wavelength of 515 nm which can operate from single pulse mode to 300 kHz. The laser is focused with a telecentric f-theta lens of 100 mm focal length. The sample position is monitored using a high precision 3D computer-controlled stage (Aerotech 3200) and a galvanometer based XY beam scanning system (SCANLAB, hurry SCAN II) controls the pulse to pulse overlap on the sample. Thermal oven (Thermoscientific Heraeus) sintering is also carried out to compare the sintering behaviour of the Ag patterns.

### 2.4. Characterization

The surface morphology is analysed with high-resolution SEM facility (Hitachi S-4700). The purpose of using an SEM is to determine if and how the sintering process leads to better connectivity between the metal NPs. To measure the variations in sheet resistance before and after sintering, the Van der Pauw method was used with a commercial four-point probe system (Ossila UK). To observe the effects of laser sintering on charge carrier mobility and concentration, the Hall measurements were performed using an Ecopia Hall Effect Measurement system (HMS-3000).

## 3. Results

### 3.1. Surface functionalization

Prior to printing, the polymer samples were subjected to argon plasma treatment for surface modifications. The exposure of plasma to a polymer surface results in the formation of radical active sites leading to an increased surface roughness and better wettability [49]. To enhance the wettability for an improved print quality, PI and clear PI bare samples are subjected to cold plasma treatment with Ar feed gas. A cold plasma is a partially ionised gas in a non-thermodynamic equilibrium state, often referred as non-thermal plasma with no or moderate increase

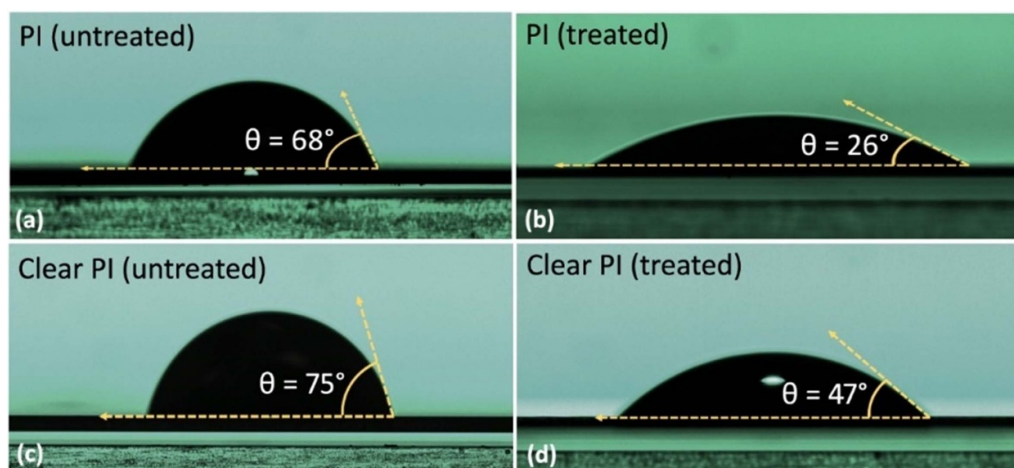


**Figure 3.** Contact angle variations before and after Ar plasma treatment of PI and clear PI substrates.

in the temperature of the gas [50]. Figure 3 shows the representative effect of plasma exposure on the substrate using contact angle measurement of deionized water on PI and clear PI before and after the treatment. The contact angle reduces from  $68^\circ$  to  $26^\circ$  on PI and from  $75^\circ$  to  $47^\circ$  on clear PI indicating that the nature of surface has become more hydrophilic due to an increase in the surface energy. The only drawback of this simple method is the short-term retainment or shelf-life of the plasma induced properties, which typically lasts for at least 3–4 d if stored properly. This fact was considered, and the printing was performed immediately after the plasma exposure. The samples were subjected to printing using PolyPico as described in the experimental section.

### 3.2. Drying and sintering of Ag NPs

After printing, the samples were dried in air at room temperature to evaporate the solvent. The complete solvent evaporation and fusing of NPs was achieved in the final step of sintering using laser and oven techniques. In this section, we first will describe the oven sintering results obtained at different settings of temperature and time. The key observations realized with femtosecond laser sintering are discussed in the later section by comparing the surface morphologies and electrical properties.

**3.2.1. Oven sintering.** Sintering of Ag NPs in an oven is a commonly adopted method due to its simplicity. Oven sintering has limitations in terms of temperatures, time, and non-selectivity of the desired region. Thermal sintering using an oven is carried out to experimentally compare the differences between femtosecond laser and oven sintering. For oven sintering, two temperature settings are selected depending on the recommendation from the ink manufacturer. The samples were heated for 20 min and 40 min at  $100^\circ\text{C}$  and  $130^\circ\text{C}$ , respectively, and the variations in the surface morphologies and electrical properties are investigated. The SEM images of all samples are provided in the supplementary information

where the selective images with best results are presented in figure 4 after a careful analysis. The size of the surface structures is estimated by using ImageJ software (<https://imagej.nih.gov/ij/>) and an average value is used to give an approximation.

Figure 4 presents the surface microstructures of untreated, oven sintered, and femtosecond laser sintered Ag NPs on photopaper (4a 1,2,3), PI (4b 1,2,3) and clear PI (4c 1,2,3) substrates, respectively. The morphology of printed Ag NPs differs depending on the substrate properties and printing parameters. The spreading of droplet and wettability of different surfaces accounts for the overall response of ink, droplet settling, stabilizing and the formation of structures during these processes. The evaporation of solvent after drying step also impacts the morphology as the outcome of drying process often compensated with cracks and defects formation. In summary, the difference in the growth of NPs on photopaper, PI and clear PI is clearly due to their different properties. For example, the surface energy of PI is higher compared to clear PI as observed in contact angle measurements. The plasma treatment was more effective on PI compared to clear PI and the droplet spreading was improved on PI.

Starting with photopaper, the morphology of untreated printed Ag NPs reflects a random distribution of particles in the form of elongated nanostructures with an average size of  $96 \pm 55$  nm (figure 4(a1)). When the NPs are sintered at  $100^\circ\text{C}$  for 20 and 40 min (figure S1-supplementary information), displacement and relocation of particles occurs. The average length of the nanostructures is increased to  $112 \pm 57$  nm for 20 min and  $120 \pm 61$  nm for 40 min respectively (figure S1). The variations in the surface morphologies are more noticeable when Ag NPs are heated at  $130^\circ\text{C}$  for 20 min on photopaper as shown in figure 4(a2). The overall orientation of NPs is random but the growth of spherically shaped particles with some interparticle attachment or necking is obtained. The average particle size improves from  $96 \pm 55$  nm to  $127 \pm 65$  nm. The particles appear bigger, and the film appears more continuous when compared to the as deposited and oven sintered film at  $100^\circ\text{C}$ . Increasing

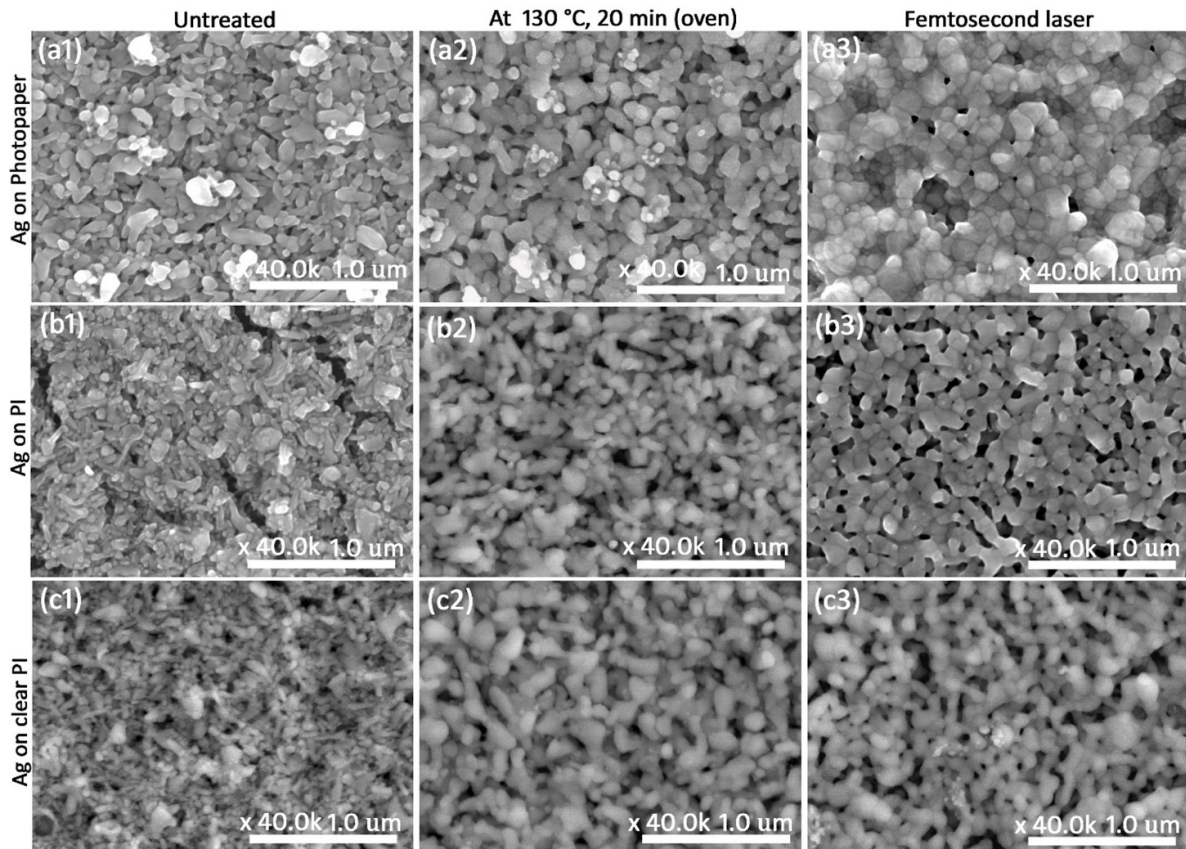


**Figure 4.** SEM images revealing the surface morphologies of Ag NPs before (a1), (b1) & (c1) and after sintering using oven at 130 °C for 20 min (a2), (b2) & (c2) and femtosecond laser (a3), (b3) & (c3), respectively.

the heating duration to 40 min at 130 °C does not appear to produce significant variations in size and connectivity when compared to samples heated for 20 min at the same temperature. Therefore, we conclude that on photopaper, oven sintering at 130 °C for 20 min is effective.

When we observe the morphology of the as printed Ag NP ink on the PI substrate, the particle distribution is the same (elongated and random), but their sizes vary as shown in figure 4(b1). Cracks or crevices are observed on dried Ag NP film on PI substrate. The appearance of cracks is often obtained during any stage for printing and post treatment process. In this instance the cracks are most likely formed due to stress relaxation caused by solvent evaporation [51]. Additionally, the properties of the ink, substrate material and their interaction play an important role in defining the formation of structures and defects such as cracks and pores. When subjected to sintering at 100 °C, the sintering effects are insignificant for 20 min and some needle like particles are only observed (figure S1). A slight increase in size and connectivity is observed when heated for 40 min (figure S1). The surface morphology of Ag NPs on PI substrate is observed to change when sintered at 130 °C for 20 min (figure 4(b2)). The calculated average size of these structures changes from  $84 \pm 40$  nm to  $121 \pm 63$  nm. Although the shape and size distribution are random, we observed an aggregation of NPs in a random manner due to sintering. The length and width of these nanostructures appears larger on completion of the thermal

treatment (figure 4(b2)). Almost a similar morphological trend is obtained when the heating duration increases to 40 min, but the size of the nanostructures reduces slightly to  $117 \pm 49$  nm (figure S1).

Thin, needle like geometry is observed for printed Ag NPs on clear PI film (figure 4(c1)). The estimated average length of these thin structures is  $72 \pm 52$  nm. The film morphology changes to somewhat circular like structures after sintering at 100 °C for 20 min. Increasing the sintering time to 40 min results in an increase in the average length ( $115 \pm 52$  nm) of the particles showing an increased continuity of the structures. Figure 4(c2) reveals the transformation of Ag NPs on clear PI after sintering at 130 °C for 20 min. The Ag NPs are converted into larger elongated structures that are well connected with a random distribution. The average length of these particles is calculated as  $130 \pm 53$  nm. Almost similar sintering effects are observed when they are heated for 40 min at 130 °C (figure S1).

Evaluating the results of oven sintering, we observed that the sintering occurred in all samples. The efficiency of sintering varies depending on the substrate and appropriate parameters. The efficient sintering region lies at higher temperature for short duration. Sintering at 130 °C for 20 min resulted in the complete sintering of Ag NPs on photopaper, PI and clear PI substrate, respectively. The particles are diffused together through the formation of a neck-like feature and finally the particle adopts a connected, elongated geometry.

**Table 3.** Variations in the size of NPs before and after femtosecond and oven sintering. The average sizes of particles are representative only and need to be considered in terms of the distribution of particles observed in each film.

Ag NPs on substrates	NP size before sintering		NP size after sintering			
	Untreated (nm)	Laser (nm)	Oven 100 (nm)		Oven 130 (nm)	
			20 min	40 min	20 min	40 min
Photopaper	96 ± 55	132 ± 51	112 ± 57	120 ± 61	127 ± 65	123 ± 60
PI	84 ± 40	128 ± 37	88 ± 33	93 ± 50	121 ± 63	117 ± 49
Clear PI	72 ± 52	125 ± 33	109 ± 67	115 ± 52	130 ± 53	128 ± 47

**3.2.2. Femtosecond laser sintering.** It is interesting to compare the sintering effects and mechanism when performed with a different sintering source, such as a femtosecond laser. The laser beam spot diameter ( $2\omega_o$ ) at the focused position ( $1/e^2$ ) and the damage threshold was calculated experimentally using Liu's method [52]. The estimated  $\omega_o$  for 515 nm laser wavelength is  $18 \mu\text{m} \pm 0.07 \mu\text{m}$ . The fluence is calculated by considering the reflection of Ag at 515 nm wavelength [53], that provides a measure of actual absorbed fluence in the material. The laser scanning parameters such as scan speed, hatch (distance between two consecutive scan lines) and laser power were optimized to obtain the sintered, conductive patterns without melting the substrates. The printed Ag samples were scanned at  $180 \text{ mm s}^{-1}$  scanning speed with  $5 \mu\text{m}$  hatching at 100 kHz resulting in 90% pulse overlapping and 10 spots per area.

Figure 4 presents the surface microstructures of untreated and femtosecond laser sintered Ag NPs on photopaper (figure 4(a3)), PI (figure 4(b3)) and clear PI (figure 4(c3)) substrates analysed with SEM. It should be noted that the SEM images are taken for the sintered samples at optimized values of the laser parameters. At first, the NPs have a random distribution with tiny, elongated structures as observed in figures 4(a1), (b1) and (c1), respectively. The random arrangement of particles is due to the presence of ink solvent and additives leaving the particles to spread on the surface. After scanning with femtosecond laser pulses, the surface morphology of Ag NPs on photopaper changes drastically and a growth of organized grains with defined boundaries is evident (figure 4(a3)). The average grain size is estimated as  $132 \pm 51 \text{ nm}$ ; the grains are less elongated after laser sintering of Ag NPs on the photopaper compared with before laser treatment. The formation of closely packed nanostructures is observed after ultrashort laser sintering. No significant melting is evident in the SEM image where the NP aggregation appears to have occurred due to compaction; joining of NPs is evident and is possibly enabled by a solid-state atomic diffusion process. This effect is compatible with ultrashort lasers where the shorter pulse duration enables the application of energy to be controlled so that insufficient heat is generated for surface melting during the pulse duration [48]. Solid-state crystallisation effects without thermal melting were observed recently for silicon, indium tin oxide, gold, and molybdenum thin film after subjecting to femtosecond laser pulses [54–57]. Comparing the variations in surface structures of Ag NPs obtained in oven and laser sintering, it is noticeable that ultrashort laser

sintering is highly effective. In oven treated samples, the variations in the shape of the surface nanostructures are insignificant but a variation in overall feature size is noticed. For femtosecond laser, the overall surface morphology has dramatically changed from irregular, random distribution to finely organized, distinct grains which are well connected.

The distribution of Ag NPs on PI follows the irregular and elongated morphologies as shown in figure 4(b1). The appearance of some cracks or gaps is noticeable within the densely distributed Ag NPs on the PI surface. After femtosecond laser treatment, the fusion of Ag NPs is apparent showing an interparticle necking with the formation of grains and the film becomes more continuous (figure 4(b3)). The overall particle size is estimated as  $128 \pm 37 \text{ nm}$  and the formation of grains is obvious. Figure 4(c3) exhibits the surface morphology of laser treated Ag NPs on clear PI substrate. While the image is less clear due to surface charging, the average length of the connected particles after femtosecond laser sintering is found to be  $125 \pm 33 \text{ nm}$ . The necking phenomenon is prominent resulting in the elongation of structures which are well connected with each other.

On comparison with oven sintered Ag NPs, the average size of the particles was enhanced after oven heating but no appreciable change in the surface structures was observed before and after heating. However, laser sintering results in organized, distinct surface features due to minimal thermal effects and a continuity between the particles appears to be realized. Although the average size of NPs is slightly higher on clear PI after heating at  $130^\circ\text{C}$ , the connectivity between the structures and electrical conductivity is higher with laser sintered samples. Therefore, we conclude that the controlling of surface structures is only possible with ultrashort laser source where thermal heating sources are not capable of controlling the structures. The estimated average particle sizes before and after oven and laser sintering are provided in table 3.

The cross-section micrographs of Ag NP films on photopaper and PI are recorded with SEM before and after femtosecond laser sintering as shown in figures 5 and 6, respectively. The spherical shape of the particles is more visible in cross section images as compared to the surface images (figure 4). The change in film morphology is also evident before and after laser sintering. The film thickness of an as-deposited Ag NP film on photopaper changes from  $950 \pm 19 \text{ nm}$  to  $1035 \pm 23 \text{ nm}$  after laser processing. The isolated Ag NPs aggregate into bigger clusters of grains by connecting the particle-to-particle grain boundaries. Similarly on PI surface,

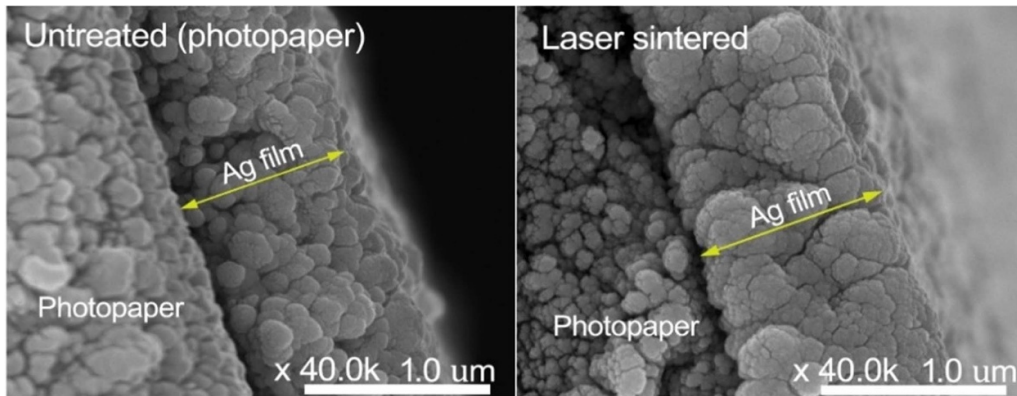


**Figure 5.** Cross section images of printed Ag NPs on photopaper revealing the variations in film morphology before and after femtosecond laser sintering.

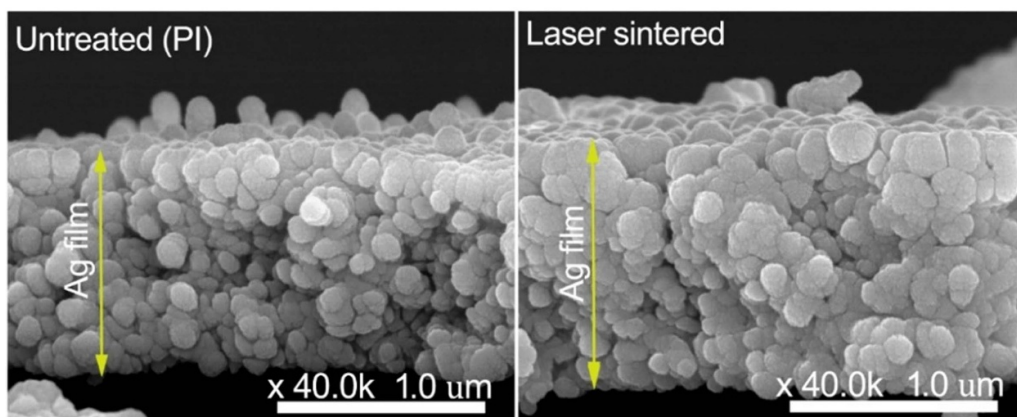


**Figure 6.** Cross section images of Ag ink on PI revealing the variations in film morphology before and after laser sintering.

the thickness of the Ag NP film is  $1094 \pm 25$  nm and improves to  $1280 \pm 27$  nm after the femtosecond laser sintering process. Upon inspecting the morphology of NP layer, clustering of NPs is observed but no appreciable melting effects are detected.

The electrical properties are closely related with microstructures of a material. Now we will discuss the impact of different sintering routes on the electrical properties of sintered Ag NPs on all three substrates which is a crucial component in printed, flexible electronics application.

### 3.3. Effect of sintering on electrical properties of Ag NPs

**3.3.1. Electrical properties- laser sintered Ag NPs.** The evidence of laser sintering and improved average particle size is clearly realized in the SEM images discussed in the previous section. Laser sintering not only improves the surface structures, but also provides better electrical properties. To observe the laser induced effects on the electrical properties of unexposed and laser sintered Ag film, the sheet resistance was measured with a commercial four-point probe system. The samples are prepared in the form of  $8 \text{ mm} \times 8 \text{ mm}$  squares to measure the sheet resistance of Ag NPs sintered on photopaper, PI and clear PI, respectively. Figure 7 presents graphs

revealing the variation in sheet resistance of Ag films as a function of laser fluence, before and after laser sintering. The sheet resistance decreases after applying laser fluence in an optimized scanning regime as evident in figure 7. The sheet resistance of as deposited Ag films on photopaper reduces from  $0.35 \pm (9.50 \times 10^{-3}) \Omega\text{Sq}^{-1}$  to  $0.13 \pm (5.80 \times 10^{-3}) \Omega\text{Sq}^{-1}$  resulting in an approximately 62% decrease in sheet resistance. For Ag films on PI, the sheet resistance changes from  $2.0 \pm (1.48 \times 10^{-3}) \Omega\text{Sq}^{-1}$  to  $0.40 \pm (1.17 \times 10^{-3}) \Omega\text{Sq}^{-1}$  resulting in an approximately 80% decreased sheet resistance. Similarly, the sheet resistance of Ag film on clear PI decreases from  $5.05 \pm (2.26 \times 10^{-3}) \Omega\text{Sq}^{-1}$  to  $0.38 \pm (5.73 \times 10^{-3}) \Omega\text{Sq}^{-1}$  providing a total of an approximately 93% decreased sheet resistance. In comparison, the highest average reduction in sheet resistance is obtained on clear PI and the overall degree of average %age reduction in sheet resistance obtained in Ag films can be written in the order as clear PI > PI > photopaper, respectively.

Figure 8 exhibits the changes in the electrical resistivity and conductivity of laser sintered Ag films calculated using the film thickness and the sheet resistance. The thickness of as-deposited Ag film is  $950 \pm 21$  nm,  $1094 \pm 28$  nm, and  $1093 \pm 39$  nm on photopaper, PI and clear PI, respectively, as measured from SEM. After laser sintering, the thickness

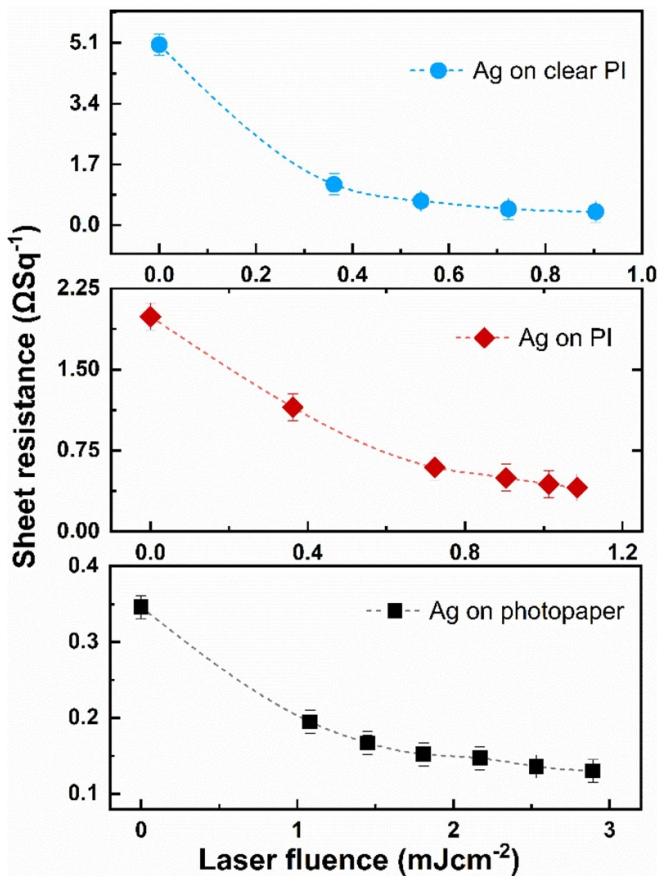


**Figure 7.** The variations in sheet resistance with laser fluence of Ag patterns printed on photopaper, PI and clear PI substrates, respectively.

changes to  $1035 \pm 43$  nm,  $1280 \pm 49$  nm and  $1278 \pm 52$  nm on photopaper, PI and clear PI respectively. The overall variations in the film thickness after laser sintering at different fluences is less significant and lies within the error values. In figure 8, with increasing laser fluence, a decreasing trend in the electrical resistivity is evident, consequently an increase in the electrical conductivity of the laser sintered films is obtained. The resistivity of untreated Ag NP film is  $3.29 \times 10^{-7} \Omega$  m,  $2.18 \times 10^{-6} \Omega$  m and  $5.53 \times 10^{-6} \Omega$  m on photopaper, PI and clear PI respectively. After femtosecond laser sintering, the resistivity reduces to a value of  $1.35 \times 10^{-7} \Omega$  m,  $4.82 \times 10^{-7} \Omega$  m and  $5.19 \times 10^{-7} \Omega$  m on photopaper, PI and clear PI substrates, respectively. The resistivity of Ag NP film on photopaper is found to be  $\sim 8.47$  times of the bulk Ag ( $1.59 \times 10^{-8} \Omega$  m). It is estimated to be as  $\approx 33$  times and  $\approx 30$  times of bulk Ag on PI and clear PI, respectively.

Hall measurements were performed on unexposed, and laser-sintered Ag films to observe the change in charge carrier concentration and mobility. The product of both parameters defines the overall electrical conductivity of a material. The carrier concentration in as-deposited Ag film on photopaper is  $3.90 \times 10^{22} \text{ cm}^{-3}$ ; this decreases to  $3.15 \times 10^{22} \text{ cm}^{-3}$  after laser sintering. This marginal change in carrier concentration is compensated by an increase in carrier mobility from

$4.42 \text{ cm}^2 \text{ V}^{-1} \text{ s}^{-1}$  to  $20.3 \text{ cm}^2 \text{ V}^{-1} \text{ s}^{-1}$ . The carrier concentration reduces from  $2.78 \times 10^{22} \text{ cm}^{-3}$  to  $1.63 \times 10^{22} \text{ cm}^{-3}$  for Ag films on PI; there is an enhancement in mobility from  $1.47 \text{ cm}^2 \text{ V}^{-1} \text{ s}^{-1}$  to  $8.89 \text{ cm}^2 \text{ V}^{-1} \text{ s}^{-1}$ . In contrast, for Ag films on clear PI, the charge carrier concentration increases from  $1.35 \times 10^{22} \text{ cm}^{-3}$  to  $2.78 \times 10^{22} \text{ cm}^{-3}$ ; the mobility is decreased from  $14.7 \text{ cm}^2 \text{ V}^{-1} \text{ s}^{-1}$  to  $12.0 \text{ cm}^2 \text{ V}^{-1} \text{ s}^{-1}$  after laser sintering. The mobility of charge carriers is influenced by the film morphology which varies with any changes in grain size, grain boundaries, lattice orientation and microstrain etc. Femtosecond laser sintering causes the formation of neck-like features between the NPs and the fusion of NPs can thus generate percolation networks for charge transport. As a result, the electron mean free path becomes larger resulting in higher charge carrier mobilities observed on photopaper and PI substrates, respectively [57]. The slight decrease in carrier mobility of Ag NPs on clear PI is unclear, it might be due to the appearance of some pores or gaps (figure 4(c3)). The difference in the continuity of sintered Ag films on three flexible substrates may possibly be caused by the variations in thermal conductivity, surface roughness and surface energy.

**3.3.2. Electrical properties- oven sintered Ag NPs.** Thermal sintering is carried out using an oven for Ag film printed on photopaper, PI and clear PI substrates, respectively. The sintering was performed at two different temperatures i.e.  $100^\circ \text{C}$  and  $130^\circ \text{C}$  for 20 min and 40 min sintering time, respectively. Figure 9 describes a comparison graph of the percentage reduction in sheet resistance in Ag NPs before and after oven and laser sintering process. When the samples are heated at  $100^\circ \text{C}$  for 20 min, the overall sheet resistance decreases by 28%, 54% and 90% for Ag films on photopaper, PI and clear PI, respectively. Increasing the sintering duration to 40 min results in 32%, 73% and 86% decrease in sheet resistance on photopaper, PI and clear PI substrates, respectively. A minor increase of +4% on photopaper and a decrease of -4% on clear PI samples is obtained. These observations reveal that the sintering of Ag NP films at a moderate temperature of  $100^\circ \text{C}$  results in conductive printed patterns.

A second set of samples was oven heated at  $130^\circ \text{C}$  for the durations of 20 min and 40 min. Percentage decrease in sheet resistance by 42%, 73% and 90% was achieved on photopaper, PI and clear PI, respectively. Similarly, when the sintering time was increased to 40 min, an average decrease in sheet resistance by 49%, 69% and 91% were obtained on photopaper, PI and clear PI substrates, respectively. The sheet resistance varies negligibly on PI and clear PI samples. The data indicates that sintering at  $100^\circ \text{C}$  for a longer time of 40 min is as effective as heating at  $130^\circ \text{C}$  for 20 min for PI samples. These findings are in correlation with SEM surface micrographs where the effective sintering with well-connected nanostructures was obtained at  $130^\circ \text{C}$  for 20 min. In summary, considering all the observations obtained for thermal sintering, we suggest sintering for 20 min at  $130^\circ \text{C}$  is effective to obtain reasonable electrical conductivities. The factor of heating time becomes less significant when the sintering temperature is higher.

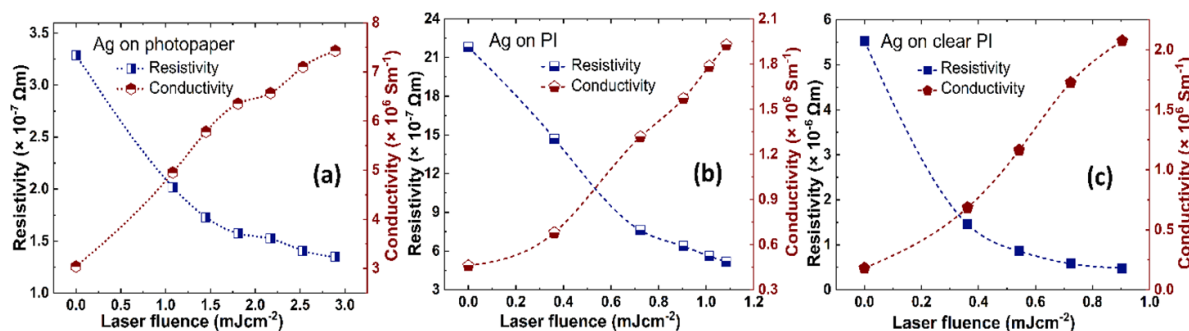


Figure 8. The variations in electrical properties of Ag films on (a) photopaper (b) PI and (c) clear PI as a function of laser fluence.

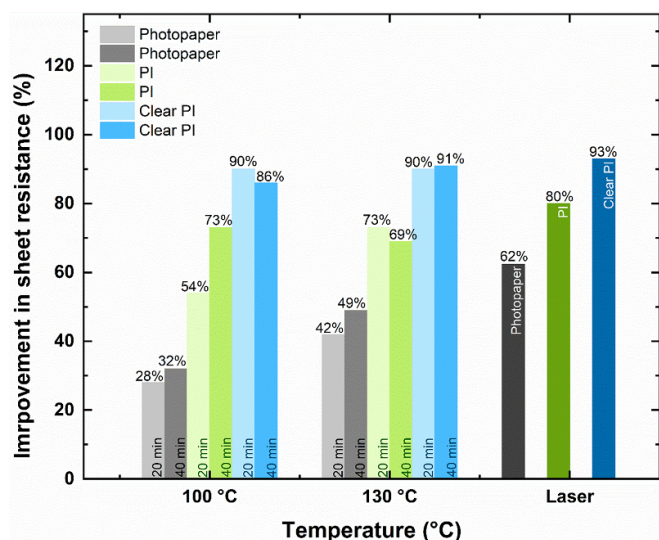


Figure 9. A comparison of percentage variation in sheet resistance of Ag NPs on photopaper, PI and clear PI after heating at 100 °C and 130 °C for 20 min and 40 min, respectively, and femtosecond laser sintering.

#### 4. Discussion

As discussed previously, room temperature, controlled printing of Ag NPs was carried out using microlitre volumes. The printing process was demonstrated on thin, flexible substrates followed by a drying and sintering process. Precise selective printing is possible for almost all types of surfaces and different patterns can be printed with high accuracy. We investigated ultrashort selective laser sintering of Ag NPs to explore the mechanism and effects involved during an ultrafast laser process in comparison to oven sintering. The effect of printing on different surfaces is also studied where it was observed that the porous nature of photopaper is important in holding the particles together during drying. This leads to good contact during sintering. On polymers, the effect appears to be different, and the impact on sintering is less clear.

Sintering is the process during which the NPs are fused together to obtain improved microstructures and grains with lower porosity. The surface area per unit volume of sintered NPs reduces due to a decrease in the total interfacial energy.

Sintering of powders is categorized into three types: solid-state sintering of crystalline materials, solid-state sintering of amorphous materials and liquid phase sintering of crystalline materials [58]. Three overlapped stages of sintering are considered in the literature categorised as an initial, intermediate, and final stage, respectively [59]. In the initial stage, a rapid neck formation and growth occurs from the contact between the neighbouring particles until the radius of the neck approaches ~40%–50% of the particle radius [60, 61]. The growth of the neck may occur due to different types of material transport including viscous flow, surface diffusion, grain boundary diffusion and volume diffusion, respectively [60]. During the intermediate stage, pore rounding and grain growth occurs, and this forms interconnected channels leading to volume expansion of the film. As the sintering proceeds, the pore channels become disconnect and isolated pores are formed with the progression of grain growth [60]. At the final stage, densification of isolated pores occurs, and the pores collapse into more compact closed spheres. At least 7%–8% of porosity is eliminated at the final stage of sintering [62]. This thermal behaviour of sintering occurs traditionally in a thermal process and has not been observed to-date in our laser sintering method.

Ultrashort laser sintering involves rather different process compared to oven sintering. Femtosecond laser pulses of 500 fs pulse duration were used to precisely sinter the printed metallic patterns with a 90% pulse overlap. Ultrashort processing has the advantage for precise low-temperature sintering as the extremely shorter pulse duration minimizes the heat-affected zone. The mechanism of laser energy absorption must be considered to understand the sintering process. When an ultrashort laser interacts with the material, photons are absorbed by conduction band electrons through photon-electron interaction. As a result, the electronic subsystem enters into an excited state with establishing higher electronic temperatures while the lattice remains unperturbed [47]. After a few femtoseconds, the electrons re-establish the Fermi-Dirac distribution during a characteristic time, i.e. the electron relaxation time required by the electrons to restore equilibrium in their energised states [48]. Initially, the excited electrons are localized within the optical penetration depth but then diffuse into deeper parts of the material due to the large temperature differences in electron and lattice systems

[63]. At picosecond timescales, the electron-phonon interactions transport the thermal energy of the electronic system to the lattice by means of electron-phonon coupling. The higher the value of the electron-phonon coupling factor, the faster the rate of energy transfer to the lattice establishing an equilibrium between the electrons and the lattice system. This is known as the two temperature model which describes the interaction of ultrashort laser pulses with a material [64, 65]. We propose that this is an efficient, controllable way to couple energy into NPs using a femtosecond laser. The transformation of randomly distributed NPs into defined, well-connected grains reveals a different sintering mechanism which we did not observe in the thermal case. The formation of connective grains is obvious in Ag film on photopaper where the overall surface morphology is changed after scanning with femtosecond laser pulses. This sintering is less clear, but the trend persists on PI and clear PI substrates, where a connected morphology of NPs appears with organized grain structures. We suggest that the sintering of Ag NPs occurred due to a solid-state atomic diffusion process in the near surface region of NPs. No evidence of melting is seen in the SEM images since the fluence is carefully controlled and the time for bulk diffusion is limited by the pulse duration. The displacement of surface-based atoms due to surface diffusion is also observed in Ag NPs when sintered with 50 fs laser pulses [66], we consider it is likely to occur here. Other non-thermal mechanisms such as weakening of interatomic bonds and lattice softening due to temporary electron emission from particles might cause the non-thermal processes to trigger the sintering of metal NPs, but this area needs further investigation. In contrast, thermal melting of NPs and coalescence is the major mechanism for nanosecond laser sintering where the characteristic time of coalescence should be at least few nanoseconds [67]. Moreover, using the femtosecond laser pulses at higher repetition rate (MHz) results in heat accumulation effects that may cause liquid-phase sintering of metal NPs with complete melting [68, 69].

We propose that ultrashort laser sintering is an efficient method to fabricate highly conductive metal NP patterns on flexible substrates without generating any deleterious heating effects. The well-defined organized growth of structures due to solid-state diffusion after femtosecond laser sintering is a key result obtained in the current study that has the potential to solve the problems encountered in thermal sintering process. The results are of key importance in order to understand laser-induced effects using femtosecond laser-enabled sintering in the visible wavelength spectral regions. We believe that this study is highly relevant in fabricating high-resolution conductive patterns on different and future heat sensitive substrates for a range of materials. This will enable the large area, selective sintering of NPs for flexible, low cost printed electronics and wearable devices with scalable manufacturing.

## 5. Conclusions

Selective laser sintering of printed Ag NPs on porous, flexible, and this substrates is carried out using femtosecond laser

pulses. The cost-effective printing of Ag NPs using micro-litre ink volumes is demonstrated on photopaper, PI and clear PI substrates at room temperature. In a carefully optimized process window, the transformation of irregular, random NPs into well defined, connected nanostructures is achieved with femtosecond laser sintering without damaging the substrate. The formation of organized surface structures is attributed to solid-state diffusion which occurs over short distances for a short period of time on or near the surface of NPs. It is best demonstrated on photopaper which localises the NP ink to the surface. Ultrashort laser sintering not only enables the formation of continuous, organized film structures but it also enhances the electrical properties. The decreased sheet resistance is estimated as 62%, 80% and 93% in Ag films on photopaper, PI and clear PI, respectively. No film/substrate damage was observed due to the near-negligible heat-affected zone of the ultrashort laser. Heating at higher temperatures of 130 °C for 20 min is useful to obtain coalesced NPs and improved conductivity. However, oven sintering is inferior to laser processing as it does not provide a control over the formation of surface microstructures. The facile, selective, and controlled printing and ultrashort laser sintering of NPs is cost-effective and offers a better control to tune the structural, as well as electrical properties of the sintered material essential for their applications.

## Data availability statement

All data that support the findings of this study are included within the article (and any supplementary files).

## Acknowledgments

This publication has emanated from research supported in part by a grant from Science Foundation Ireland under Grant No. 16/RC/3872. For the purpose of Open Access, the author has applied public copyright license to any Author Accepted Manuscript version arising from this submission. The authors gratefully acknowledge the SEM facility provided by The Centre for Microscopy and Imaging at University of Galway and their support and assistance in this work.

## Conflict of interest

The authors have no conflicts to disclose.

## ORCID iDs

Ayesha Sharif  <https://orcid.org/0000-0001-5604-1475>  
Nazar Farid  <https://orcid.org/0000-0003-0556-6794>  
Mingqing Wang  <https://orcid.org/0000-0003-1933-1566>  
Rajani K Vijayaraghavan  <https://orcid.org/0000-0003-1096-448X>  
Asim Jilani  <https://orcid.org/0000-0001-5451-2050>  
Gabriel Leen  <https://orcid.org/0000-0003-2448-4428>

## References

- [1] Strambeanu N *et al* 2015 Nanoparticles: definition, classification and general physical properties *Nanoparticles' Promises and Risks* (Berlin: Springer) pp 3–8
- [2] Akbari B, Tavandashi M P and Zandrahimi M 2011 Particle size characterization of nanoparticles—a practical approach *Iran. J. Mater. Sci. Eng.* **8** 48–56 (available at: <http://ijmse.iust.ac.ir/article-1-341-en.html>)
- [3] Guo D, Xie G and Luo J 2013 Mechanical properties of nanoparticles: basics and applications *J. Phys. D: Appl. Phys.* **47** 013001
- [4] Khan I, Saeed K and Khan I 2019 Nanoparticles: properties, applications and toxicities *Arab. J. Chem.* **12** 908–31
- [5] Phan H T and Haes A J 2019 What does nanoparticle stability mean? *J. Phys. Chem. C* **123** 16495–507
- [6] Bouafia A, Laouini S E, Ahmed A S A, Soldatov A V, Algarni H, Feng Chong K and Ali G A M 2021 The recent progress on silver nanoparticles: synthesis and electronic applications *Nanomaterials* **11** 2318
- [7] Tran Q H and Le A-T 2013 Silver nanoparticles: synthesis, properties, toxicology, applications and perspectives *Adv. Nat. Sci.* **4** 033001
- [8] Ahamed M, AlSalhi M S and Siddiqui M 2010 Silver nanoparticle applications and human health *Clin. Chim. Acta* **411** 1841–8
- [9] Carbone M, Donia D T, Sabbatella G and Antiochia R 2016 Silver nanoparticles in polymeric matrices for fresh food packaging *J. King Saud Univ. Sci.* **28** 273–9
- [10] Kokura S *et al* 2010 Silver nanoparticles as a safe preservative for use in cosmetics *Nanomed. Nanotechnol. Biol. Med.* **6** 570–4
- [11] Nie X, Wu S, Liao S, Chen J, Huang F, Li W, Wang Q and Wei Q 2021 Light-driven self-disinfecting textiles functionalized by PCN-224 and Ag nanoparticles *J. Hazard. Mater.* **416** 125786
- [12] Ramalingam V 2022 *Silver Nanoparticles for Biomedical Applications, in Nanoparticle Therapeutics* (Amsterdam: Elsevier) pp 359–75
- [13] Xu L, Wang Y-Y, Huang J, Chen C-Y, Wang Z-X and Xie H 2020 Silver nanoparticles: synthesis, medical applications and biosafety *Theranostics* **10** 8996
- [14] Dhand V, Soumya L, Bharadwaj S, Chakra S, Bhatt D and Sreedhar B 2016 Green synthesis of silver nanoparticles using Coffea arabica seed extract and its antibacterial activity *Mater. Sci. Eng. C* **58** 36–43
- [15] Ravindran A, Chandran P and Khan S S 2013 Biofunctionalized silver nanoparticles: advances and prospects *Colloids Surf. B* **105** 342–52
- [16] Kalantari K, Mostafavi E, Afifi A M, Izadiyan Z, Jahangirian H, Rafiee-Moghaddam R and Webster T J 2020 Wound dressings functionalized with silver nanoparticles: promises and pitfalls *Nanoscale* **12** 2268–91
- [17] Choudhury H *et al* 2020 Silver nanoparticles: advanced and promising technology in diabetic wound therapy *Mater. Sci. Eng. C* **112** 110925
- [18] Wiklund J, Karakoç A, Palko T, Yiğitler H, Ruttik K, Jäntti R and Paltakari J 2021 A review on printed electronics: fabrication methods, inks, substrates, applications and environmental impacts *J. Manuf. Mater. Process.* **5** 89
- [19] Mola G T, Mthethwa M C, Hamed M S G, Adedeji M A, Mbuyise X G, Kumar A, Sharma G and Zang Y 2021 Local surface plasmon resonance assisted energy harvesting in thin film organic solar cells *J. Alloys Compd.* **856** 158172
- [20] Sangno R, Maity S and Mehta R 2016 Plasmonic effect due to silver nanoparticles on silicon solar cell *Proc. Comput. Sci.* **92** 549–53
- [21] Ji S Y, Choi W, Kim H-Y, Jeon J-W, Cho S-H and Chang W 2018 Fully solution-processable fabrication of multi-layered circuits on a flexible substrate using laser processing *Materials* **11** 268
- [22] Abdolmaleki H, Kidmose P and Agarwala S 2021 Droplet-based techniques for printing of functional inks for flexible physical sensors *Adv. Mater.* **33** 2006792
- [23] Dimitriou E and Michailidis N S 2021 Printable conductive inks used for the fabrication of electronics: an overview *Nanotechnology* **32** 502009
- [24] Turan N, Saeidi-Javash M, Chen J, Zeng M, Zhang Y and Go D B 2021 Atmospheric pressure and ambient temperature plasma jet sintering of aerosol jet printed silver nanoparticles *ACS Appl. Mater. Interfaces* **13** 47244–51
- [25] Leen G 2016 A new pico-litre fluid dispensing technology for new possibilities *Biosens. J.* **5** 1000139
- [26] Leen G and Bryce B 2016 *Liquid Droplet Dispenser US9387492B2* (available at: <https://patents.google.com/patent/US9387492B2/en>)
- [27] Bourassa J, Ramm A, Feng J Q and Renn M J 2019 Water vapor-assisted sintering of silver nanoparticle inks for printed electronics *SN Appl. Sci.* **1** 1–6
- [28] Rajan K, Roppolo I, Chiappone A, Bocchini S, Perrone D and Chiolerio A 2016 Silver nanoparticle ink technology: state of the art *Nanotechnol. Sci. Appl.* **9** 1
- [29] Sowade E, Kang H, Mitra K Y, Weiß O J, Weber J and Baumann R R 2015 Roll-to-roll infrared (IR) drying and sintering of an inkjet-printed silver nanoparticle ink within 1 second *J. Mater. Chem. C* **3** 11815–26
- [30] Niittynen J, Abbel R, Mäntysalo M, Perelaer J, Schubert U S and Lupo D 2014 Alternative sintering methods compared to conventional thermal sintering for inkjet printed silver nanoparticle ink *Thin Solid Films* **556** 452–9
- [31] Moon Y J, Kang H, Kang K, Moon S-J and Young Hwang J 2015 Effect of thickness on surface morphology of silver nanoparticle layer during furnace sintering *J. Electron. Mater.* **44** 1192–9
- [32] Mo L, Guo Z, Yang L, Zhang Q, Fang Y, Xin Z, Chen Z, Hu K, Han L and Li L 2019 Silver nanoparticles based ink with moderate sintering in flexible and printed electronics *Int. J. Mol. Sci.* **20** 2124
- [33] Lee D J, Park S H, Jang S, Kim H S, Oh J H and Song Y W 2011 Pulsed light sintering characteristics of inkjet-printed nanosilver films on a polymer substrate *J. Micromech. Microeng.* **21** 125023
- [34] Wünscher S, Stumpf S, Teichler A, Pabst O, Perelaer J, Beckert E and Schubert U S 2012 Localized atmospheric plasma sintering of inkjet printed silver nanoparticles *J. Mater. Chem.* **22** 24569–76
- [35] Ma S, Bromberg V, Liu L, Egitto F D, Chiarot P R and Singler T J 2014 Low temperature plasma sintering of silver nanoparticles *Appl. Surf. Sci.* **293** 270–15
- [36] Tan H W, Saengchairat N, Goh G L, An J, Chua C K and Tran T 2020 Induction sintering of silver nanoparticle inks on polyimide substrates *Adv. Mater. Technol.* **5** 1900897
- [37] Munir Z A, Quach D V and Ohyanagi M 2011 Electric current activation of sintering: a review of the pulsed electric current sintering process *J. Am. Ceram. Soc.* **94** 1–19
- [38] Liu W, An R, Wang C, Zheng Z, Tian Y, Xu R and Wang Z 2018 Recent progress in rapid sintering of nanosilver for electronics applications *Micromachines* **9** 346
- [39] Roy N K, Dibua O G, Jou W, He F, Jeong J, Wang Y and Cullinan M A 2018 A comprehensive study of the sintering of copper nanoparticles using femtosecond, nanosecond, and continuous wave lasers *J. Micro Nano-Manuf.* **6** 010903
- [40] Ko S H, Pan H, Grigoropoulos C P, Luscombe C K, Fréchet J M J and Poulidakos D 2007 Air stable high resolution organic transistors by selective laser sintering of ink-jet printed metal nanoparticles *Appl. Phys. Lett.* **90** 141103

- [41] Liu Q, Xu B, Zhang Y, Wang X, Mei X and Wang X 2021 Picosecond laser sintering of silver paste printed by laser induced forward transfer *Opt. Laser Technol.* **135** 106712
- [42] Maekawa K, Yamasaki K, Niizeki T, Mita M, Matsuba Y, Terada N and Saito H 2012 Drop-on-demand laser sintering with silver nanoparticles for electronics packaging *IEEE Trans. Compon. Packaging Manuf. Technol.* **2** 868–77
- [43] Mu B, Wang X, Zhang X and Xiao X 2022 Laser direct sintering approach for additive manufacturing in flexible electronic *Results Eng.* **13** 100359
- [44] Ko S H, Pan H, Grigoropoulos C P, Luscombe C K, Fréchet J M J and Poulidakos D 2007 All-inkjet-printed flexible electronics fabrication on a polymer substrate by low-temperature high-resolution selective laser sintering of metal nanoparticles *Nanotechnology* **18** 345202
- [45] Hernandez-Castaneda J C, Lok B K and Zheng H 2020 Laser sintering of Cu nanoparticles on PET polymer substrate for printed electronics at different wavelengths and process conditions *Front. Mech. Eng.* **15** 303–18
- [46] Liu S, Yuen M C, White E L, Boley J W, Deng B, Cheng G J and Kramer-Bottiglio R 2018 Laser sintering of liquid metal nanoparticles for scalable manufacturing of soft and flexible electronics *ACS Appl. Mater. Interfaces* **10** 28232–41
- [47] Gamaly E G 2011 *Femtosecond Laser-Matter Interaction: Theory, Experiments and Applications* (Jenny Stanford Publishing)
- [48] Jiang L and Tsai H-L 2005 Improved two-temperature model and its application in ultrashort laser heating of metal films *ASME. J. Heat Transfer* **127** 1167–73
- [49] Vesel A and Mozetic M 2017 New developments in surface functionalization of polymers using controlled plasma treatments *J. Phys. D: Appl. Phys.* **50** 293001
- [50] Law V J, Chebbi A and O'Neill F T 2013 Resonances and patterns within the kINPen-MED atmospheric pressure plasma jet *Chaos 2013 Chaotic Modeling and Simulation Int. Conf. at Istanbul Turkey* vol 1 (CMSIM)
- [51] Liu S et al 2019 Structure inheritance in nanoparticle ink direct-writing processes and crack-free nano-copper interconnects printed by a single-run approach *Materials* **12** 1559
- [52] Liu J M 1982 Simple technique for measurements of pulsed Gaussian-beam spot sizes *Opt. Lett.* **7** 196–8
- [53] Yang H U, D'Archangel J, Sundheimer M L, Tucker E, Boreman G D and Raschke M B 2015 Optical dielectric function of silver *Phys. Rev. B* **91** 235137
- [54] Farid N, Brunton A, Rumsby P, Monaghan S, Duffy R, Hurley P, Wang M, Choy K-L and O'Connor G M 2021 Femtosecond laser-induced crystallization of amorphous silicon thin films under a thin molybdenum layer *ACS Appl. Mater. Interfaces* **13** 37797–808
- [55] Sharif A, Farid N, Wang M, Vijayaraghavan R K, Choy K-L, McNally P J and O'Connor G M 2021 Non-melt selective enhancement of crystalline structure in molybdenum thin films using femtosecond laser pulses *J. Appl. Phys.* **55** 115301
- [56] Sharif A, Farid N, Vijayaraghavan R K, McNally P J and O'Connor G M 2021 Femtosecond laser assisted crystallization of gold thin films *Nanomaterials* **11** 1186
- [57] Farid N, Sharif A, Vijayaraghavan R K, Wang M, Chan H, Brunton A, McNally P J, Choy K L and O'Connor G M 2021 Improvement of electrical properties of ITO thin films by melt-free ultra-short laser crystallization *J. Appl. Phys.* **54** 185103
- [58] Bordia R K, Kang S J L and Olevsky E A 2017 Current understanding and future research directions at the onset of the next century of sintering science and technology *J. Am. Ceram. Soc.* **100** 2314–52
- [59] Frenkel J 1945 Viscous flow of crystalline bodies under the action of surface tension *J. Phys.* **9** 385
- [60] Kang S-J L 2004 *Sintering: Densification, Grain Growth and Microstructure* (Amsterdam: Elsevier)
- [61] Rahaman M N 2017 *Ceramic Processing and Sintering* (Boca Raton, FL: CRC Press)
- [62] Fang Z Z 2010 *Sintering of Advanced Materials* (Amsterdam: Elsevier) (<https://doi.org/10.1002/adma.200903147>)
- [63] Fujimoto J, Liu J M, Ippen E P and Bloembergen N 1984 Femtosecond laser interaction with metallic tungsten and nonequilibrium electron and lattice temperatures *Phys. Rev. Lett.* **53** 1837
- [64] Rethfeld B, Ivanov D S, Garcia M E and Anisimov S I 2017 Modelling ultrafast laser ablation *J. Phys. D: Appl. Phys.* **50** 193001
- [65] Anisimov S, Kapeliovich B and Perelman T 1974 Electron emission from metal surfaces exposed to ultrashort laser pulses *Zh. Eksp. Teor. Fiz.* **66** 375–7
- [66] Noh J, Ha J and Kim D 2020 Femtosecond and nanosecond laser sintering of silver nanoparticles on a flexible substrate *Appl. Surf. Sci.* **511** 145574
- [67] Pan H, Ko S H and Grigoropoulos C 2008 The coalescence of supported gold nanoparticles induced by nanosecond laser irradiation *Appl. Phys. A* **90** 247–53
- [68] Cheng C-W, Chang C-L, Chen J-K and Wang B 2018 Femtosecond laser melting of silver nanoparticles: comparison of model simulations and experimental results *Appl. Phys. A* **124** 1–8
- [69] Cheng C-W and Chen J 2016 Femtosecond laser sintering of copper nanoparticles *Appl. Phys. A* **122** 1–8